JOURNAL OF COMPUTATIONAL PHYSICS 39, 137–163 (1981)

Nonlinear Water Wave Generation Using the Method of Lines

SAMUEL OHRING

David W. Taylor Naval Ship Research and Development Center, Bethesda, Maryland 20084

Received October 31, 1979; revised February 26, 1980

The method of lines is applied to the two-dimensional nonlinear water wave generation resulting from the abrupt acceleration from rest to constant speed of a pressure distribution on the surface of initially calm water. The surface pressure distribution can be viewed as modeling the air cushion pressure of a surface effect ship. Steady state at the craft is achieved for all cases computed, most of which are highly nonlinear and which exhibit sharp downstream wave crests that approach the limiting sharpness of the Stokes wave for steady irrotational gravity waves. Computations show pronounced sharpening of wave crests, broadening of wave troughs, and shortening of wavelengths compared to linear theory. Wave resistance, rates of work, and energy are computed. Computer time is saved by applying the method of lines in a local neighborhood of the free surface in combination with a standard Laplace solver below. Results are presented.

1. INTRODUCTION

Various methods [1, 2] have been used in the numerical computation of nonlinear water waves. These methods, including both transient and steady state modeling, successfully calculate waves with moderately steep slopes but encounter inaccuracy or, in the transient case, instability when the wave slopes become very steep. The objective of the present study was to calculate very steep waves, possibly up to the point of breaking, using the method of lines.

The method of lines involves discretization of the governing partial differential equation except in one dependent variable. An example of a physical application is given in [3]. In this paper the method of lines is applied as used by G. H. Meyer [4, 5], who has applied it to several physical problems (not water wave problems, however) involving a nonlinear free boundary, that is, a boundary whose shape is not known in advance and at which a nonlinear boundary condition is applied. Meyer's method resembles a successive line overrelaxation iteration procedure. In such a procedure all quantities on a line (the coordinate direction with respect to which derivatives are not discretized and which intersects the free surface) are computed (including free surface values) given the latest values on adjacent lines. A successive Gauss–Seidel line iteration procedure was used in this paper and worked nicely. In this paper the method of lines is applied only on a grid imbedding the free surface. This imbedding grid solution (on and below the free surface) is made to interact in a

0021-9991/81/010137-27$02.00/0

convergent manner with the solution of Laplace's equation (obtained by sucessive point overrelaxation in this paper) on a much larger grid below and slightly overlapping the imbedding grid.

The method of lines has two main numerical components: (1) the solution of a nonlinear ordinary differential equation, and (2) the solution of a small nonlinear system of simultaneous equations (on the order of 2 or 3). As mentioned in [4], recent advances in the solution to each component make the method of lines attractive. It is easily programmable and extendable to three dimensions compared to other physical space methods. However, the method has a high arithmetic operation count and is therefore computationally slower than most other methods.

The two-dimensional moving surface pressure distribution problem, which has been studied by von Kerczek and Salvesen [6] and also by Haussling and Van Eseltine [2], is considered a test problem. The surface pressure distribution can be viewed as simulating the air cushion pressure of a surface effect ship. In this paper a transient approach to steady state at the craft is used since it seems the most natural way to compute two- and three-dimensional nonlinear free surface flows (i.e., one computes the nonlinear free surface until a steady state is achieved at the craft well before waves reach the downstream computational boundary). The transient approach has been used [7] to compute 3-D linear steady state ship waves. This approach removes the difficulty of dealing with the nonlinear free surface downstream boundary condition which is not known. Von Kerckzek and Salvesen [1] used a steady state 2-D method which uses a stream function formulation and is therefore not applicable to 3-D problems. In [2] a transient approach was used. For truly time dependent problems, obviously a transient approach is necessary.

Although a body is not present in the moving surface pressure distribution problem, problems with bodies should offer no additional difficulties for the method of lines since the body boundary condition is much simpler than the nonlinear free surface condition which is the chief concern in this paper. Meyer [4, 5] has successfully obtained solutions for nonlinear free boundary problems (not involving water waves) with bodies in polar coordinates.

Numerical results obtained in this paper are compared with linear analytic solutions, with the limiting Stokes solution [8] for steady irrotational gravity waves and with features predicted by the perturbation analysis of Salvesen [9] for nonlinear water waves. The numerical results show pronounced sharpening of wave crests, broadening of wave troughs, and shortening of the wavelength compared to linear theory. In addition, wave resistance and time rates of work and energy are computed.

In Section 2 of this paper the formulation of the moving surface pressure distribution problem is given. This is followed in Section 3 by a description of the numerical method employed. In Section 4 results obtained with the numerical method are given. Section 5 summarizes conclusions drawn from the results.

2. The 2-D Surface Pressure Distribution Problem

In a Cartesian coordinate reference frame moving to the left with the surface pressure distribution (Fig. 1a) the following initial boundary value problem is considered:

$$\eta_t = -\eta_x(1+\phi_x) + \phi_y \qquad \text{at} \quad y = \eta, \tag{1}$$

$$\phi_t = -\eta/\mathrm{Fr}^2 - \phi_x - \tfrac{1}{2}(\phi_x^2 + \phi_y^2) - \delta p/\mathrm{Fr}^2 \qquad \text{at} \quad y = \eta, \tag{2}$$

$$\phi_{xx} + \phi_{yy} = 0 \qquad \text{for} \quad 0 \leqslant x \leqslant L_1,\ -h \leqslant y \leqslant \eta, \tag{3}$$

$$\phi_x = 0 \qquad \text{at} \quad x = 0, L_1, \tag{4}$$

$$\phi_y = 0 \qquad \text{at} \quad y = -h, \tag{5}$$

$$\text{at } t = 0; \qquad \phi = 0 \text{ everywhere}, \tag{6}$$

$$\eta = -\delta p, \tag{7}$$

$$\text{with } p = \sin^2[\pi(x - x_0)], \qquad x_0 \leqslant x \leqslant x_0 + 1, \tag{8}$$

$$p = 0, \qquad x < x_0,\ x > x_0 + 1. \tag{9}$$

The origin of the Cartesian coordinate reference frame is in the undisturbed free surface. It is assumed that the flow is irrotational and that the fluid is incompressible. It is also assumed that the surface elevation can be described at any time t by specifying y as a single-valued function of x: $y = \eta(x, t)$. Equations (1) and (2) are, respectively, the kinematic and dynamic boundary conditions at the free surface. Initially the pressure distribution is at rest over a motionless fluid and is then accelerated impulsively to a constant speed U. The formulation presented here applies

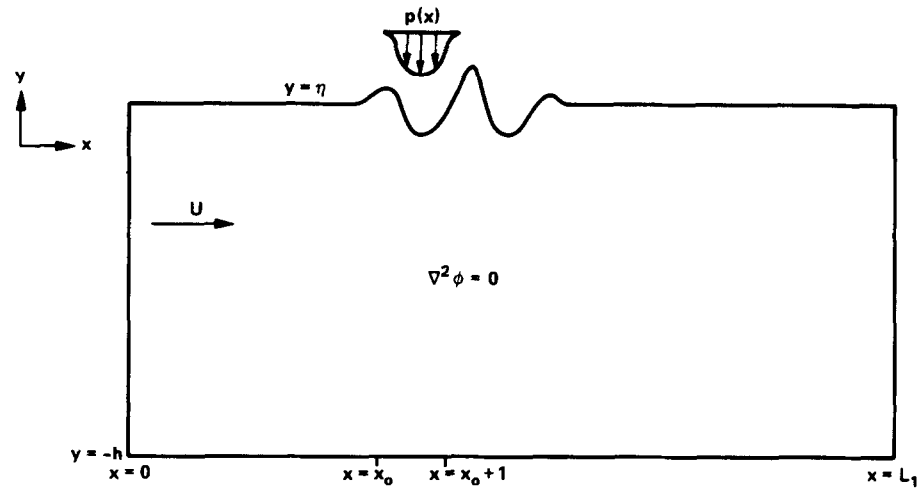

FIG. 1a. The computational region in the reference frame fixed to the moving pressure distribution.

to this particular problem, but the formulation and numerical method used in this paper can easily be extended to handle more general accelerations. The variables have been nondimensionalized in Eqs. (1) through (9) as follows,

$$(x', y') = L(x, y) \qquad t' = \frac{L}{U} t,$$
$$\phi' = LU\phi, \qquad p' = Pp, \qquad \eta' = L\eta, \tag{10}$$

where primes denote dimensional variables, $\phi(x, y, t)$ is the velocity potential relative to a nonmoving reference frame, p is pressure, P is the maximum pressure in the surface distribution, and L is the length of the surface pressure distribution. The dimensionless parameters are $\mathrm{Fr} = U/\sqrt{gL}$, the Froude number based on L, and $\delta = P/\rho gL$. The gravitational acceleration is denoted by g and ρ is the constant density. The parameter δ can be regarded as the ratio of two length scales. The length $P/\rho g$ is the hydrostatic surface displacement caused by the surface pressure P. The initial surface elevation in Eq. (7) is the hydrostatic displacement due to the pressure disturbance. The parameter δ is a measure of the strength of the pressure distribution. Note that the initial conditions of Eqs. (6) and (7) are equivalent mathematically to the relation

$$\phi_t = 0 \qquad \text{at } t = 0 \quad \text{at } y = \eta. \tag{11}$$

Figure 1b shows initial surface elevations at t = 0 for five δ's considered later in this paper. The problem represented by Eqs. (1) through (9) can be linearized with

$$\eta_t = -\eta_x + \phi_y,$$
$$\phi_t = -\phi_x - \eta/\mathrm{Fr}^2 - \delta p/\mathrm{Fr}^2, \qquad \text{at} \quad y = 0, \tag{12}$$

replacing Eqs. (1) and (2). This linearized problem often provides sufficient accuracy when wave slopes are small.

Formulas for the kinetic and potential energies of the fluid, the time rate of work performed by the pressure on the fluid, and the wave resistance experienced by the pressure to its movement across the fluid are, respectively,

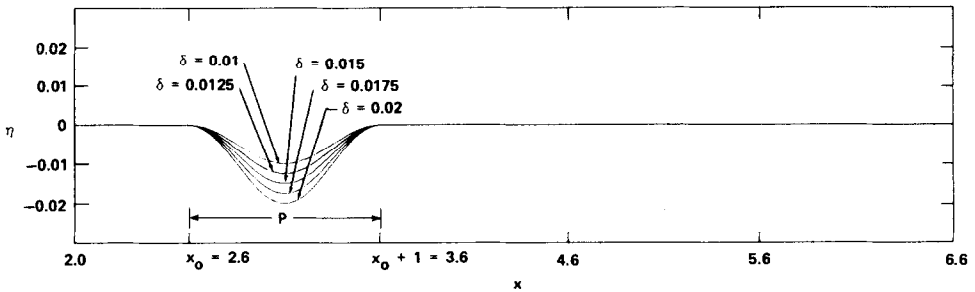

FIG 1b. Initial surface elevations at $t = 0$ for $\delta = 0.01$, 0.0125, 0.015, 0.0175, 0.02.

$$KE = \frac{1}{2}\int [\phi(\phi_y - \phi_x \eta_x)]_{y=\eta}\, dx, \tag{13}$$

$$PE = \frac{1}{2\mathrm{Fr}^2}\int \eta^2\, dx, \tag{14}$$

$$\dot{W} = \frac{\delta}{\mathrm{Fr}^2}\int [p(\phi_x \eta_x - \phi_y)]_{y=\eta}\, dx, \tag{15}$$

$$C_R = -\frac{\delta}{\mathrm{Fr}^2}\int p(y=\eta)\,\eta_x\, dx. \tag{16}$$

The kinetic and potential energies have been nondimensionalized with respect to $\rho L^2 U^2$ and the wave resistance by $\rho L U^2$. The total energy of the field is then expressed by $E = KE + PE$. Energy conservation is represented by the relation

$$\dot{W} = dE/dt. \tag{17}$$

It follows from Eqs. (1), (15), and (16) that at steady state

$$C_R = \dot{W}. \tag{18}$$

3. The Numerical Method

Consider an overlapping grid system as shown in Fig. 2 for the computational region of Fig. 1a. The grid for $0 \leqslant x \leqslant L_1$, $y_0 \leqslant y \leqslant y_m$ is that used by the method of lines. The grid for $0 \leqslant x \leqslant L_1$, $-h \leqslant y \leqslant y_1$ is that used by a Laplace equation solver

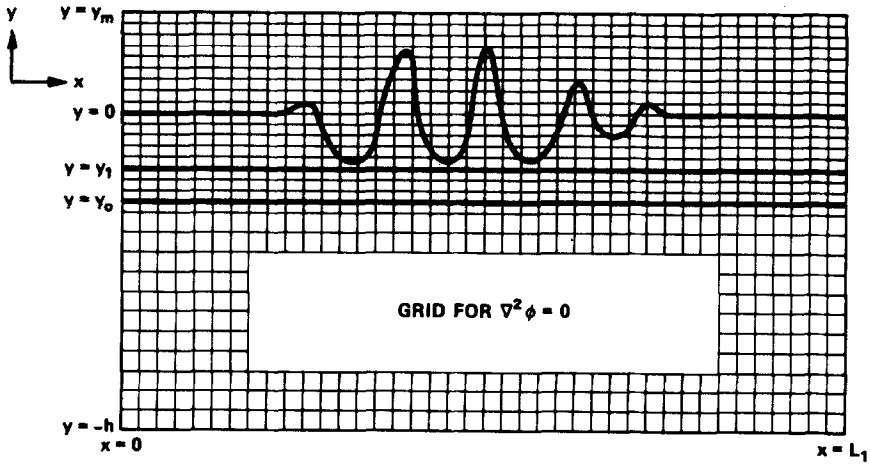

FIG. 2. Overlapping grid system for the computational region.

which in this paper was Gauss–Seidel point successive overrelaxation, although a fast direct method [10] could be used. However, the major part of the computing time is used by the method of lines and this is the reason for confining it to the upper grid. The solutions on the two overlapping grids are made to interact in a convergent iterative process to be described. Note from Fig. 2 that the upper grid extends beyond the free surface, this extension being available if needed. Essentially, the grid only up to the free surface (as it is generated) is used in the computational process.

On the upper grid the initial boundary value problem of Eqs. (1) through (9) is spatially finite differenced in x only, with second-order central differencing replacing derivatives in the x-direction. Briefly, the overall computational scheme for obtaining a solution at time level t^{n+1} in the computational region of Fig. 2 from a computed solution at t^n (with time step $\Delta t = t^{n+1} - t^n$) is as follows.

Proceeding in the upper grid on the ith iteration pass ($i = 1$ initially) from the upstream end, ($x = 0$) in Fig. 2, to the downstream end at $x = L_1$, the ith iterate solution of Eqs. (1) through (3) (subject to a Dirichlet condition at y_0) at each line x_j (Fig. 3) is solved based on the ith iterate solution at x_{j-1} and the $i-1$st iterate solution at x_{j+1}. The solution at t^n is taken as the 0th iterate solution. After this ith sweep in the upper grid, Eq. (3) is solved (here by Gauss–Seidel successive overrelaxation) in the lower grid subject to Eqs. (4), (5) and a Dirichlet condition at $y = y_1$ represented by $\phi^{(i)}(x_j, y_1, t^{n+1})$ (all x_j), where the superscript (i) refers to the ith iteration. This yields at y_0 the value $\phi^{(i)}(x_j, y_0, t^{n+1})$ (all x_j) as a new Dirichlet condition for the upper grid. This completes the ith computational cycle. Before the $(i+1)$st computational cycle with an $(i+1)$st iteration sweep in the upper grid is started, the following convergence criteria are applied for all x_j:

$$\begin{aligned} |\eta^{(i)}(x_j, t^{n+1}) - \eta^{(i-1)}(x_j, t^{n+1})| &< \varepsilon_1, \\ |\phi^{(i)}(x_j, y_0, t^{n+1}) - \phi^{(i-1)}(x_j, y_0, t^{n+1})| &< \varepsilon_2. \end{aligned} \tag{19}$$

If the convergence criteria are satisfied, the ith iterate solution in the entire computational region (Fig. 2) is taken as the solution at t^{n+1}. If the convergence

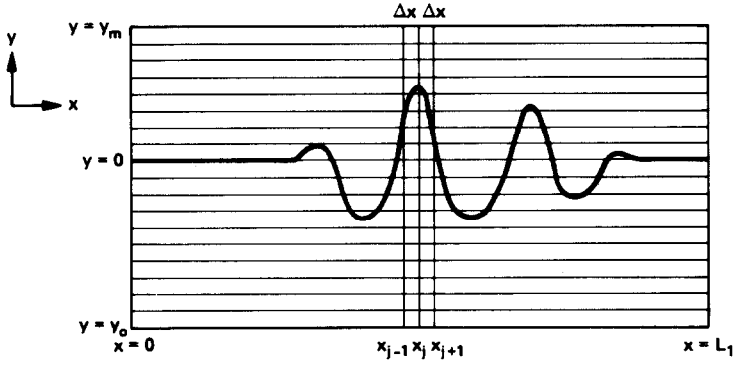

FIG. 3. The neighboring grid of the vertical line x_j.

criteria are not satisfied, the $(i+1)$st computational cycle and, if necessary, additional computational cycles are computed until the convergence criteria are satisfied.

The present computational scheme is a modification of that used by Meyer [4, 5], who applies the method of lines to entire computational regions. The method of lines requires significant computer time, but because the present scheme employs the method of lines only in a grid strip containing the free surface, the amount of computer time is significantly reduced.

The following discussion will now be confined to the upper grid and, in particular, to the ith iterate solution for time level t^{n+1} at the line $x = x_j$ as in Fig. 3.

An implicit time differencing scheme known as Euler's modified method is used for the free surface Eqs. (1) and (2). An implicit scheme has been chosen instead of an explicit scheme because in general it is more stable and can use much larger time steps. The author is not aware of any explicit time advancement scheme having been used successfully in a nonlinear free surface problem. One gets, at the line x_j,

$$-\eta^{(i)}(x_j, t^{n+1}) + \eta(x_j, t^n) + (\Delta t/2)[F^{(i)}_{n+1} + F_n] = 0, \tag{20}$$

$$-\phi^{(i)}(x_j, \eta^{(i)}(x_j, t^{n+1}), t^{n+1}) + \phi(x_j, \eta(x_j, t^n), t^n) + (\Delta t/2)[G^{(i)}_{n+1} + G_n] = 0, \tag{21}$$

where $F^{(i)}_{n+1}$, $G^{(i)}_{n+1}$ are

$$F^{(i)}_{n+1} = \frac{-(\eta^{(i-1)}(x_{j+1}, t^{n+1}) - \eta^{(i)}(x_{j-1}, t^{n+1}))}{2\,\Delta x}(1 + \phi^{(i)}_x(x_j, \eta^{(i)}(x_j, t^{n+1}), t^{n+1})) + \phi^{(i)}_y(x_j, \eta^{(i)}(x_j, t^{n+1}), t^{n+1}), \tag{22}$$

$$G^{(i)}_{n+1} = -\eta^{(i)}(x_j, t^{n+1})/\mathrm{Fr}^2 - \delta p/\mathrm{Fr}^2 - \phi^{(i)}_x(x_j, \eta^{(i)}(x_j, t^{n+1}), t^{n+1}) - \tfrac{1}{2}([\phi^{(i)}_y(x_j, \eta^{(i)}(x_j, t^{n+1}), t^{n+1})]^2 + [\phi^{(i)}_x(x_j, \eta^{(i)}(x_j, t^{n+1}), t^{n+1})]^2) + \phi^{(i)}_y(x_j, \eta^{(i)}(x_j, t^{n+1}), t^{n+1})\, F^{(i)}_{n+1} \tag{23}$$

with

$$\phi^{(i)}_x(x_j, \eta^{(i)}(x_j, t^{n+1}), t^{n+1}) = \frac{\phi^{(i-1)}(x_{j+1}, \eta^{(i)}(x_j, t^{n+1}), t^{n+1}) - \phi^{(i)}(x_{j-1}, \eta^{(i)}(x_j, t^{n+1}), t^{n+1})}{2\,\Delta x}.$$

F_n and G_n are also given by the right sides of Eqs. (22) and (23), respectively, with t^n replacing t^{n+1} and with all iteration superscripts (i) and $(i-1)$ removed. An extra term $\phi^{(i)}_y(x_j, \eta^{(i)}(x_j, t^{n+1}), t^{n+1})\, F^{(i)}_{n+1}$ has been added to $G^{(i)}_{n+1}$ (and the corresponding term added to G_n), since the local derivative ϕ_t in Eq. (2) has been replaced by a substantive derivative approximated by

$$(\phi(x_j, \eta(x_j, t^{n+1}), t^{n+1}) - \phi(x_j, \eta(x_j, t^n), t^n))/\Delta t.$$

When the ith iterate solution at the line x_j, is computed, all dependent variables on lines other than x_j (such as $\phi^{(i)}$, $\eta^{(i)}$ at x_{j-1} and $\phi^{(i-1)}$, $\eta^{(i-1)}$ at x_{j+1}) are known and the solution at t^n is known on all lines.

Since the free surface $y = \eta(x, t)$ does not ordinarily lie on grid points (x_j, y_k), the terms $\phi^{(i-1)}(x_{j+1}, \eta^{(i)}(x_j, t^{n+1}), t^{n+1})$, $\phi^{(i)}(x_{j-1}, \eta^{(i)}(x_j, t^{n+1}), t^{n+1})$ are expressed as linear functions of the unknown $\eta^{(i)}(x_j, t^{n+1})$ (in terms of known values $\phi^{(i-1)}(x_{j+1}, y_k, t^{n+1})$ nearest the free surface $\eta^{(i-1)}(x_{j+1}, t^{n+1})$ and known values $\phi^{(i)}(x_{j-1}, y_k, t^{n+1})$ nearest the free surface $\eta^{(i)}(x_{j-1}, t^{n+1})$, respectively).

The unknowns in Eqs. (20) and (21) are therefore $\eta^{(i)}(x_j, t^{n+1})$, $\phi^{(i)}(x_j, \eta^{(i)}(x_j, t^{n+1}), t^{n+1})$, and $\phi_y^{(i)}(x_j, \eta^{(i)}(x_j, t^{n+1}), t^{n+1})$. Another equation is required so that these three unknowns may be solved from the resulting system of simultaneous nonlinear equations. This additional equation will be supplied from the consideration of Laplace's equation (Eq. (3)).

Using central differencing for Eq. (3) about a point (x_j, y_k) on the line x_j gives

$$\phi_{yy}^{(i)}(x_j, y_k, t^{n+1}) = 2\phi^{(i)}(x_j, y_k, t^{n+1})/(\Delta x)^2 - [\phi^{(i-1)}(x_{j+1}, y_k, t^{n+1}) + \phi^{(i)}(x_{j-1}, y_k, t^{n+1})]/(\Delta x)^2. \quad (24)$$

Since the last term in Eq. (24) is assumed known, one has a simple second-order ordinary differential equation for $\phi^{(i)}$ at x_j for y at successive intervals $[y_k, y_{k+1}]$. Over each such interval $\phi^{(i)}$ has an analytic solution given in terms of a linear combination of exponential functions of y plus a linear function of y (if the last term in Eq. (24) is replaced by a linear function of y based on assumed known values of $\phi^{(i-1)}(x_{j+1}, y_k, t^{n+1})$, $\phi^{(i)}(x_{j-1}, y_k, t^{n+1})$ at all $y = y_k$). Thus, one could proceed to solve Eq. (24) by sweeping upward along the line $x = x_j$ starting at $y = y_0$ (Fig. 2) where starting conditions for both ϕ and ϕ_y (i.e., $\phi^{(i-1)}(x_j, y_0, t^{n+1})$, $\phi_y^{(i-1)}(x_j, y_0, t^{n+1})$) must be given. Solving Eq. (24) in this way would give a solution independent of the free surface conditions (Eqs. (20), (21)). Such independence cannot be permitted. It is also quite obvious that Eq. (24) cannot be solved by sweeping downward from a free surface unknown in advance. What is required is a scheme which (1) uncouples the free surface conditions from the integration of the ordinary differential equations representing the Laplace equation (3) along lines $x = x_j$ and (2) calculates a solution which satisfies both the free surface equations and Laplace's equation.

Following Meyer's method [4], which fulfills these needs and which is outlined here for completeness of the discussion, one considers the Ricatti transformation that relate ϕ and ϕ_y through auxiliary variables $R(x, y)$, $W(x,y)$:

$$\phi^{(i)}(x_j, y, t^{n+1}) = R(x_j, y)\,\phi_y^{(i)}(x_j, y, t^{n+1}) + W(x_j, y). \quad (25)$$

(The continuous variable y has replaced the grid ordinate y_k. The same will be true of Eq. (24) in the following discussion.) Substituting Eq. (25) for $\phi^{(i)}(x_j, y, t^{n+1})$ in Eq. (24) gives

$$\phi_{yy}^{(i)}(x_j, y, t^{n+1}) = (2/(\Delta x)^2)\, R(x_j, y)\, \phi_y^{(i)}(x_j, y, t^{n+1})$$
$$- [\phi^{(i)}(x_{j-1}, y, t^{n+1}) + \phi^{(i-1)}(x_{j+1}, y, t^{n+1}) - 2W(x_j, y)]/(\Delta x)^2, \quad (26)$$

a first order differential equation for ϕ_y along the line x_j once $R(x_j, y)$, $W(x_j, y)$ are known (values on adjacent lines are assumed known). To obtain R and W, Eq. (25) is differentiated with respect to y. The resulting equation will be a first order ordinary differential equation for W along the line x_j (after substituting Eq.(26) for $\phi_{yy}^{(i)}(x_j, y, t^{n+1})$) if and only if R satisfies

$$R_y(x_j, y) = 1 - (2/(\Delta x)^2)\, R^2(x_j, y), R(x_j, y_0) = 0. \quad (27)$$

The equation for W is

$$W_y(x_j, y) = -(2/(\Delta x)^2)\, R(x_j, y)\, W(x_j, y) + R(x_j, y)[\phi^{(i-1)}(x_{j+1}, y, t^{n+1})$$
$$+ \phi^{(i)}(x_{j-1}, y, t^{n+1})]/(\Delta x)^2, W(x_j, y_0) = \phi^{(i-1)}(x_j, y_0, t^{n+1}). \quad (28)$$

The initial conditions for R and W in Eqs. (27) and (28), respectively, arise from Eq. (25) and the known initial Dirichlet condition for $\phi^{(i-1)}(x_j, y_0, t^{n+1})$ (obtained from the Laplace equation solution on the lower grid (Fig. 2)).

The computation along the line x_j (at consecutive y_k) in the upper grid (Figs. 2 and 3) from $y = y_0$ to $y = \eta^{(i)}(x_j, t^{n+1})$ proceeds as follows. Given $R(x_j, y_0)$ and $W(x_j, y_0)$, one obtains R and W from Eqs. (27) and (28), respectively. Equation (27) has an analytical solution for R:

$$R(y) = [(\Delta x)\, e^{(2)^{3/2}(y-y_0)/\Delta x} - (\Delta x)]/[\sqrt{2} + \sqrt{2}\, e^{(2)^{3/2}(y-y_0)/\Delta x}]. \quad (29)$$

R is actually independent of x_j and is a function of y and the parameters y_0 and Δx. Since R is analytically known, the numerical solution to Eq. (28) for W is obtained first, with the solution being advanced successively over intervals $[y_k, y_{k+1}]$ in the positive y-direction on the line x_j from y_0 to the first y_k beyond the latest known iterate value of $y = \eta$, which is $\eta^{(i-1)}(x_j, t^{n+1})$. The term $[\phi^{(i-1)}(x_{j+1}, y, t^{n+1}) + \phi^{(i)}(x_{j-1}, y, t^{n+1})]$ in Eq. (28) (which is known at $y = y_k, y_{k+1}$ for each interval) is expressed as a linear function over $[y_k, y_{k+1}]$, based on its values at the endpoints of the interval.

At the unknown free surface $y = \eta^{(i)}(x_j, t^{n+1})$, Eq. (25) can be expressed as

$$\phi^{(i)}(x_j, \eta^{(i)}(x_j, t^{n+1}), t^{n+1}) = R(x_j, \eta^{(i)}(x_j, t^{n+1}))\, \phi_y^{(i)}(x_j, \eta^{(i)}(x_j, t^{n+1}), t^{n+1})$$
$$+ W(x_j, \eta^{(i)}(x_j, t^{n+1})). \quad (30)$$

R and W can now be expressed as functions of $\eta^{(i)}(x_j, t^{n+1})$ (W is expressed

as a linear function of $\eta^{(i)}(x_j, t^{n+1})$ based on its computed grid values in the immediate neighborhood of the free surface). Equation (30) will be the third nonlinear equation in addition to Eqs. (20) and (21) with unknowns $\eta^{(i)}(x_j, t^{n+1})$, $\phi^{(i)}(x_j, \eta^{(i)}(x_j, t^{n+1}), t^{n+1})$, $\phi_y^{(i)}(x_j, \eta^{(i)}(x_j, t^{n+1}), t^{n+1})$. The unknown $\phi_y^{(i)}(x_j, \eta^{(i)}(x_j, t^{n+1}), t^{n+1})$ can be expressed directly in terms of the unknowns $\eta^{(i)}(x_j, t^{n+1})$, $\phi^{(i)}(x_j, \eta^{(i)}(x_j, t^{n+1}), t^{n+1})$ from Eq. (20). This expression for $\phi_y^{(i)}(x_j, \eta^{(i)}(x_j, t^{n+1}), t^{n+1})$ is substituted in Eqs. (21) and (30) and it is these two equations which are solved simultaneously for $\eta^{(i)}(x_j, t^{n+1})$, $\phi^{(i)}(x_j, \eta^{(i)}(x_j, t^{n+1}), t^{n+1})$. Newton's method has been used here.

The computed value of $\phi_y^{(i)}(x_j, \eta^{(i)}(x_j, t^{n+1}), t^{n+1})$ serves as a starting condition for the numerical solution of Eq. (26) for $\phi_y^{(i)}$ along the line x_j. The numerical solution advances from $y = \eta^{(i)}(x_j, t^{n+1})$ to $y = y_0$ along grid points on x_j. The first grid interval from $y = \eta^{(i)}(x_j, t^{n+1})$ to the first fixed grid point just below will be of variable size depending on the value of $\eta^{(i)}(x_j, t^{n+1})$. The term $[\phi^{(i)}(x_{j-1}, y, t^{n+1}) + \phi^{(i-1)}(x_{j+1}, y, t^{n+1}) - 2W(x_j, y)]$ in Eq. (26) is expressed as a linear function over each interval $[y_k, y_{k+1}]$ based on its values at the endpoints of the interval.

The velocity potential $\phi^{(i)}(x_j, y, t^{n+1})$ at grid points along the line x_j from $y = \eta^{(i)}(x_j, t^{n+1})$ to $y = y_0$ is then obtained from Eq. (25).

The numerical solutions of Eqs. (28) and (26) for W and ϕ_y, respectively, are accomplished by using a second order Runge–Kutta method [11] (a "predictor–corrector" method) for each successive grid interval $[y_k, y_{k+1}]$. Given an initial condition for the dependent variable at one endpoint of the interval, the dependent variable is solved for at the other endpoint of the grid interval and serves as the initial condition for the next interval. Solutions are obtained for each successive interval $[y_k, y_{k+1}]$ since terms (previously discussed) in the right sides of Eqs. (26) and (28) have been expressed as linear functions over each such interval. This is especially desireable when the free surface lies within the interval $[y_k, y_{k+1}]$.

When $x_j = 0$ or L_1 where Eq. (4) applies, or when central differencing for unequal intervals about the line x_j is applied, Eqs. (20), (21), and (25) through (28) are modified but are solved in the same manner. This completes the discussion of the ith iterate solution for time level t^{n+1} at the line x_j in the upper grid.

The Cartesian grid used in this paper for Fig. 2 is defined as follows: Proceeding from $x = 0$, which is considered the line x_1, x_j is defined as

$$
\begin{aligned}
&x_j = (j-1)\,\Delta x, && \Delta x = 0.085, && j = 2, 3, \ldots, 11;\\
&x_j = x_{11} + (j-11)\,\Delta x, && \Delta x = 0.065, && j = 12, 13, \ldots, 21;\\
&x_j = x_{21} + (j-21)\,\Delta x, && \Delta x = 0.05, && j = 22, 23, \ldots, 31;\\
&x_j = x_{31} + (j-31)\,\Delta x, && \Delta x = 0.04, && j = 32, 33, \ldots, 146;\\
&x_j = x_{146} + (j-146)\,\Delta x, && \Delta x = 0.05, && j = 147, 148, \ldots, 166;\\
&x_j = x_{166} + (j-166)\,\Delta x, && \Delta x = 0.0714, && j = 167, 168, \ldots, 173;\\
&x_j = x_{173} + (j-173)\,\Delta x, && \Delta x = 0.1, && j = 174, 175, \ldots, 188.
\end{aligned}
$$

Proceeding from $y = -h$ in the positive y-direction, y_k is

$$\begin{aligned} y_k &= -h + (k-1)\,\Delta y, && \Delta y = 0.04, \quad k = 2, 3, \ldots, 26; \\ y_k &= y_{26} + (k-26)\,\Delta y, && \Delta y = 0.03, \quad k = 27, 28, \ldots, 31; \\ y_k &= y_{31} + (k-31)\,\Delta y, && \Delta y = 0.02, \quad k = 32, 33, \ldots, 36; \\ y_k &= y_{36} + (k-36)\,\Delta y, && \Delta y = 0.01, \quad k = 37, 38, \ldots, 56. \end{aligned} \tag{32}$$

With this grid definition, $L_1 = 9.5998$, $h = 1.35$ and $y_m = 0.1$. The values $y_1 = -0.07$ and $y_0 = -0.1$ were used in Fig. 2. Note that the symbol y_1 has a special meaning and is not involved in the definition of Eq. (32). In Eqs. (8) and (9), $x_0 = 2.6$ so that the pressure distribution of Eq. (8) was located from $x_j = 46$ through $x_j = 71$. The time step used was $\Delta t = 0.03$. In Eqs. (19) the values for ε_1 and ε_2 were $\varepsilon_1 = \varepsilon_2 = 0.0002$.

During the computer runs for the cases to be discussed under Results, an instability develops in time at the free surface just upstream of the pressure distribution. This has been noticed also in previous numerical work on nonlinear water wave problems [2]. This situation was controlled in the present study with a light application to the free surface in this upstream region of a filtering function due to Shapiro [13] which removes the shortest wavelength errors. This filtering has been used successfully by Longuet-Higgins and Cokelet [12] on a breaking wave problem. To be precise the second-order filtering function used was

$$\hat{f}_j = (1/16)[-(f_{j-2} + f_{j+2}) + 4(f_{j-1} + f_{j+1}) + 10 f_j], \tag{33}$$

where the subscripts refer to functional evaluations at $x_{j\pm2}$, $x_{j\pm1}$, x_j. After each iteration sweep through the computational region, $\phi^{(i)}(x_j, \eta^{(i)}(x_j, t^{n+1}), t^{n+1})$ and $\eta^{(i)}(x_j, t^{n+1})$ at x_j for $j = 43, 44, \ldots, 51$ were replaced as follows,

$$\begin{aligned} &\phi^{(i)}(x_j, \eta^{(i)}(x_j, t^{n+1}), t^{n+1}) \\ &\quad \leftarrow (1 - 0.1(j-42))\,\hat{\phi}_j + 0.1(j-42)\,\phi^{(i)}(x_j, \eta^{(i)}(x_j, t^{n+1}), t^{n+1}), \\ &\eta^{(i)}(x_j, t^{n+1}) \leftarrow (1 - 0.1(j-42))\,\hat{\eta}_j + 0.1(j-42)\,\eta^{(i)}(x_j, t^{n+1}), \end{aligned} \tag{34}$$

where $\hat{\phi}_j$, $\hat{\eta}_j$ are given by the expression for $\hat{f}_j$ in Eq. (33), with the functional values on the right-hand side of Eq. (33) given respectively by $\phi^{(i)}(x_j, \eta^{(i)}(x_j, t^{n+1}), t^{n+1})$ and $\eta^{(i)}(x_j, t^{n+1})$ at $j \pm 2, j \pm 1, j$. Upstream for $j = 1$ to $j = 42$ only $\hat{\phi}_j$, $\hat{\eta}_j$ were used (after each iteration sweep) where the free surface is expected to be flat with $\eta = 0$. It is to be emphasized that filtering was not used anywhere else on the free surface.

4. Results

The following seven cases have been computed on the Texas Instruments Advanced Scientific Computer at the Naval Research Laboratory, Washington, D.C.:

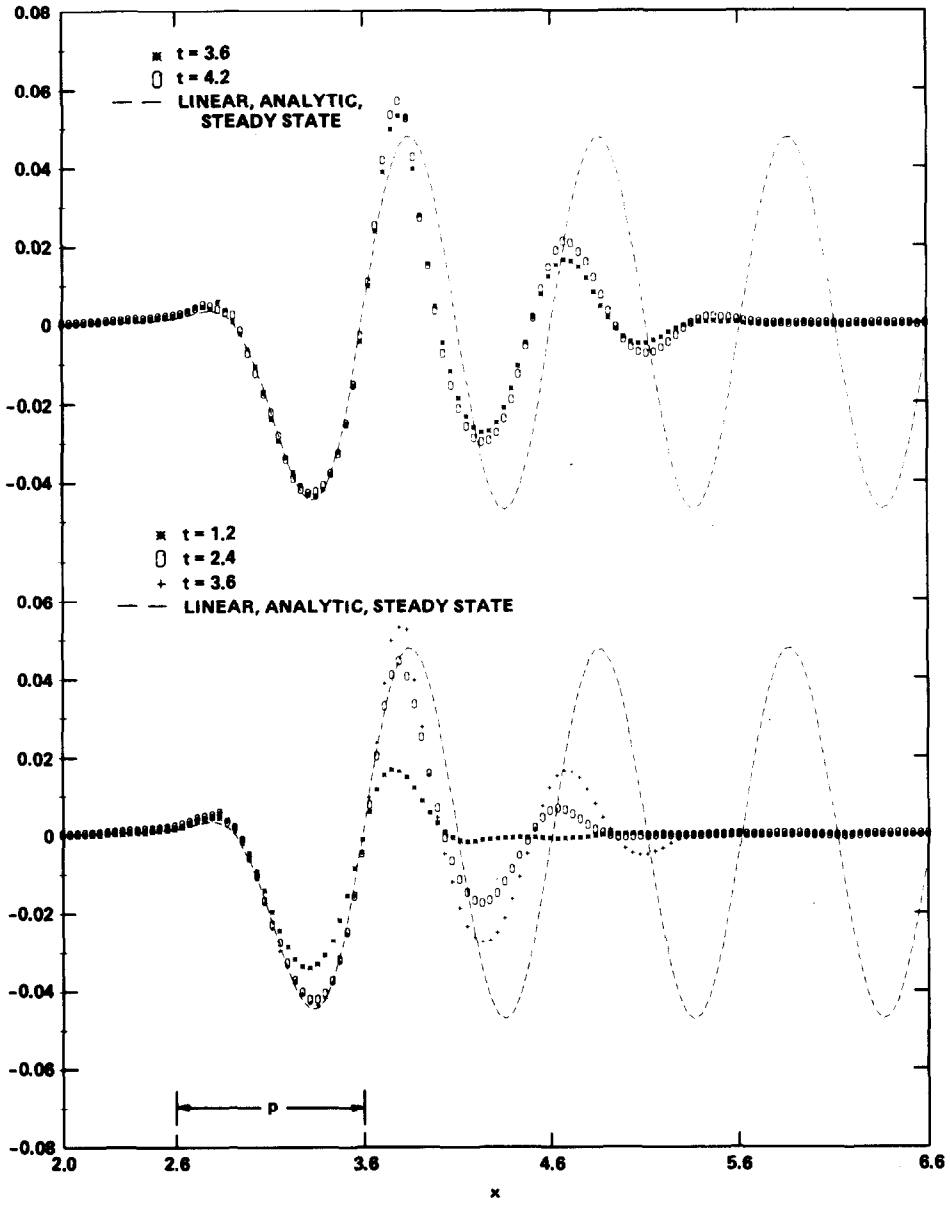

FIG. 4. Time sequence of waves generated for $\mathrm{Fr} = 0.4$, $\delta = 0.015$.

$$\text{Fr} = 0.4, \qquad \delta = 0.01, 0.0125, 0.015, 0.0175, 0.02,$$

$$\text{Fr} = 0.45, \qquad \delta = 0.015,$$

$$\text{Fr} = 0.35, \qquad \delta = 0.0125.$$

In discussing the results for these cases, the numerical solutions will be compared with the analytic solution for the linearized, steady state version of the free surface problem given by Eqs. (1) through (9). This linearized version of the problem is given by Eqs. (12) with time derivatives omitted, Eq. (3) applied on a region of infinite depth with $\phi = 0$ at $y = -\infty$, and with no surface waves far upstream of the pressure distribution given by Eqs. (8) and (9). While numerical solutions for the nonlinear problem were computed on the region of Fig. 1a with a depth h equal to 1.35, it is valid to compare these numerical solutions with solutions obtained on regions of infinite depth. This is true since a depth of 1.35 is considerably greater than half the wavelength for all cases considered (see Stoker [14]) and therefore bottom effects are negligible.

The analytic solution [6, 15], for η for the linearized, steady state problem just described is given by

$$\eta(x) = \frac{\delta}{\pi \text{Fr}^2} \int_{-\infty}^{\infty} ds\, p(s)\, \text{Re}\, I\{i(x-s)/\text{Fr}^2\}, \tag{35}$$

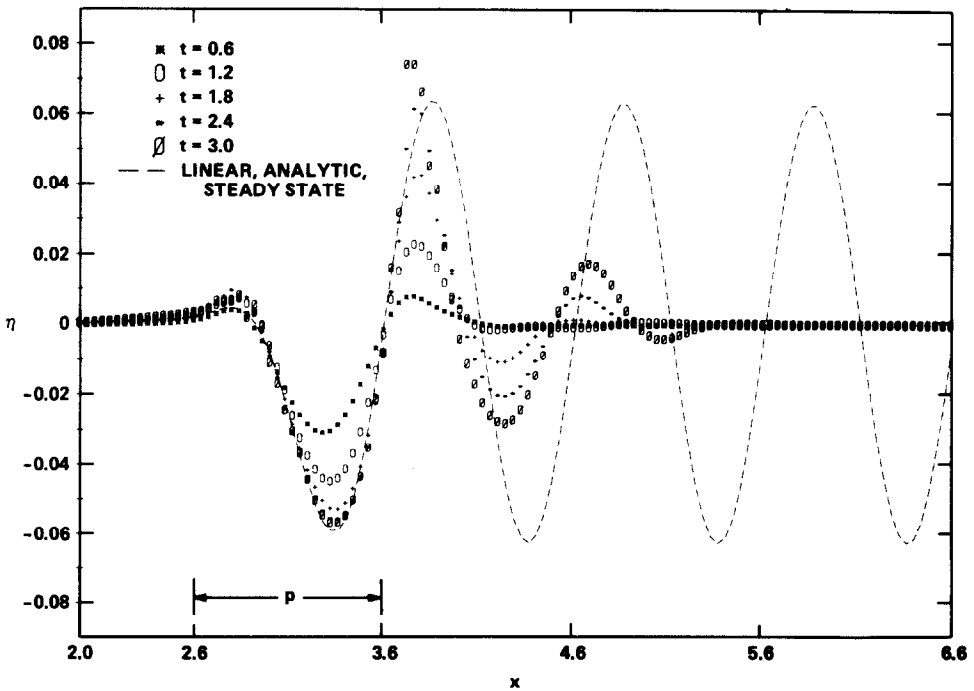

FIG. 5. Time sequence of waves generated for $\text{Fr} = 0.4$, $\delta = 0.02$.

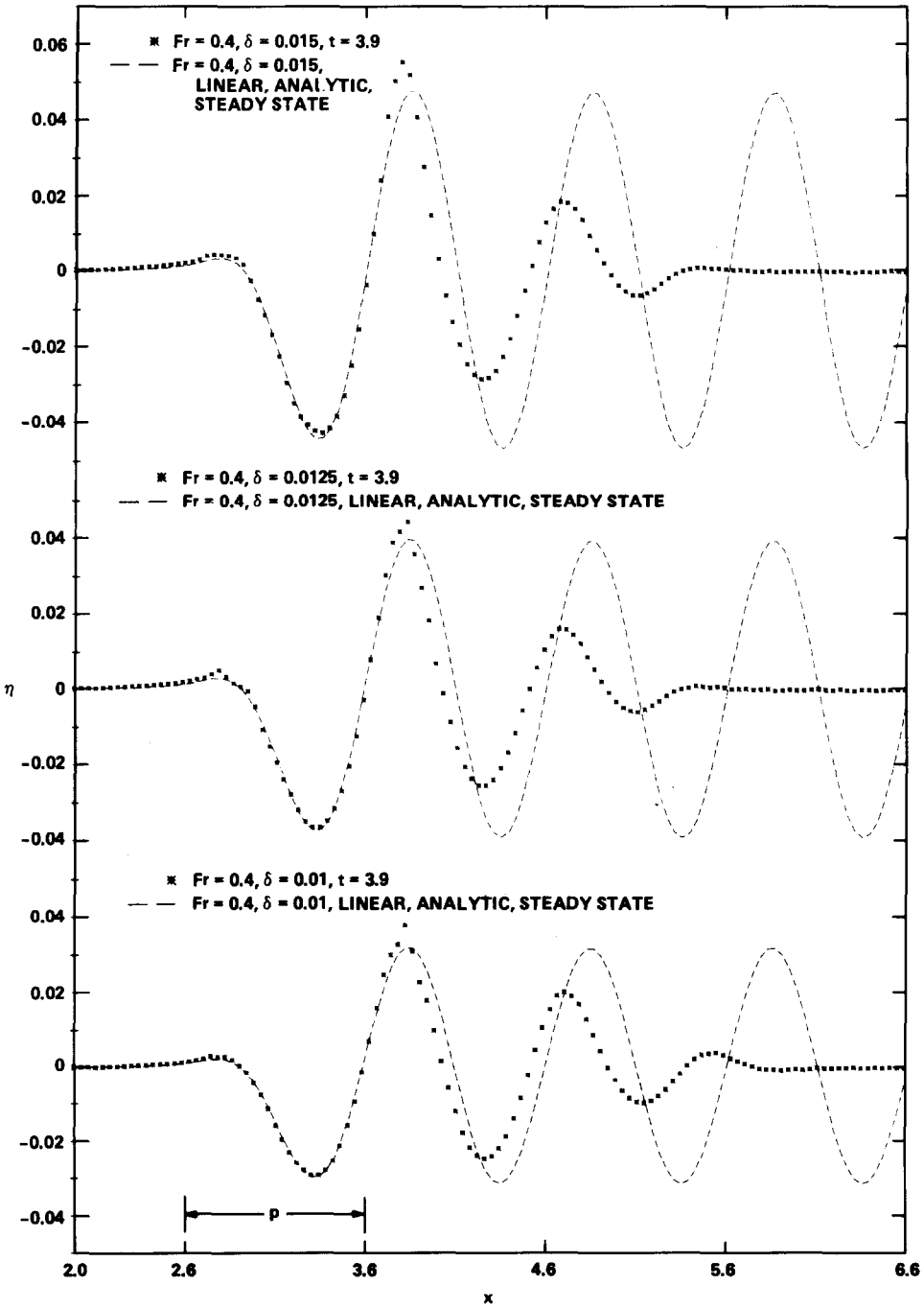

FIG. 6. Late time wave profiles for Fr = 0.4 with $\delta = 0.01$, 0.0125, 0.015, 0.0175, and 0.02.

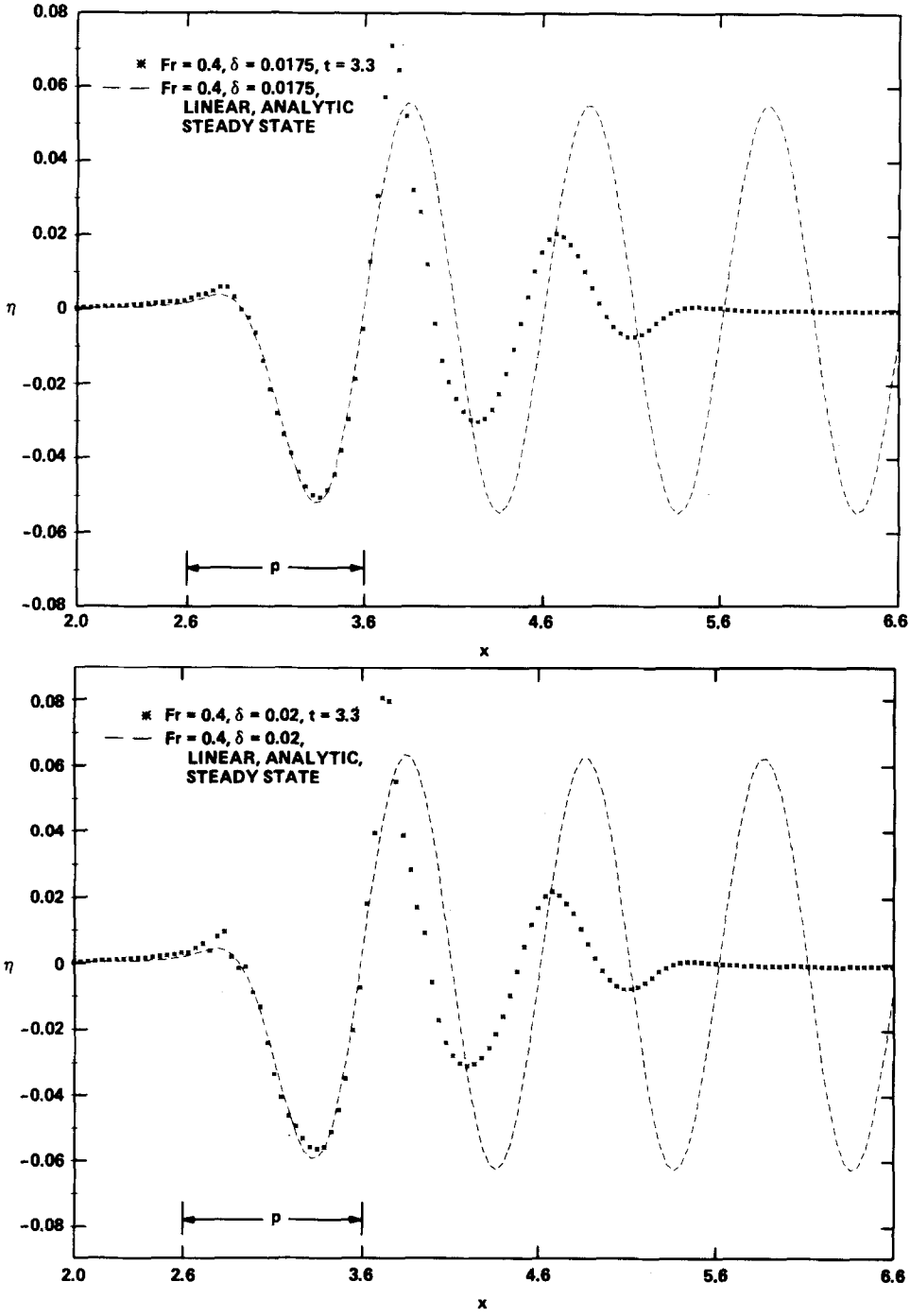

FIG. 6—*Continued.*

where the complex function $I(\zeta)$ is defined in terms of the exponential integral as

$$I(\zeta) = e^{-\zeta} \int_{-\zeta}^{\infty} \frac{e^{-v}}{v}\, dv = e^{-\zeta} \left(-\gamma - \ln \zeta + i\pi - \sum_{n=1}^{\infty} \frac{\zeta^n}{nn!} \right), \tag{36}$$

where γ is Euler's constant.

The analytic coefficient of wave resistance C_R, defined by Eq. (16) for the linearized, steady state problem with finite depth [16], is given by

$$C_R = \frac{\delta^2}{\mathrm{Fr}^6} \left[\frac{K^2[S^2 + Q^2]}{1 - (h/\mathrm{Fr}^2)\,\mathrm{sech}^2(hK/\mathrm{Fr}^2)} \right] \tag{37}$$

with

$$\begin{matrix} S \\ Q \end{matrix} = \int p \begin{matrix} \cos \\ \sin \end{matrix} (Kx/\mathrm{Fr}^2)\, dx,$$

where K is the nonzero positive root of $K - \tanh(hK/\mathrm{Fr}^2) = 0$. Note that δ appears only as a constant factor outside the integral sign in Eq. (35) and that the analytic C_R of Eq. (37) is a linear function of δ^2.

Figure 4 shows waves generated in time for the case $\mathrm{Fr} = 0.4$, $\delta = 0.015$. This and all following figures to be discussed have been computer drawn using the Tektronix 4014-1 graphics terminal and Calcomp 936 plotter. During each time unit the pressure distribution moves upstream (to the left) a distance equal to the length of the distribution. The pressure distribution (Eq. (8)), which is applied at the free surface in this and all following figures, is shown located at $2.6 \leqslant x \leqslant 3.6$. In Fig. 4 the development of a wave train downstream is apparent, with a steady state wave profile at the pressure distribution at $t = 3.6$ (the pressure distribution has moved 3.6 of its lengths upstream to the left). The first wave crest downstream of the pressure distribution appears to be at almost steady state at $t = 4.2$. Note that the numerical solution for this and all of the following cases shows the typical nonlinear wave

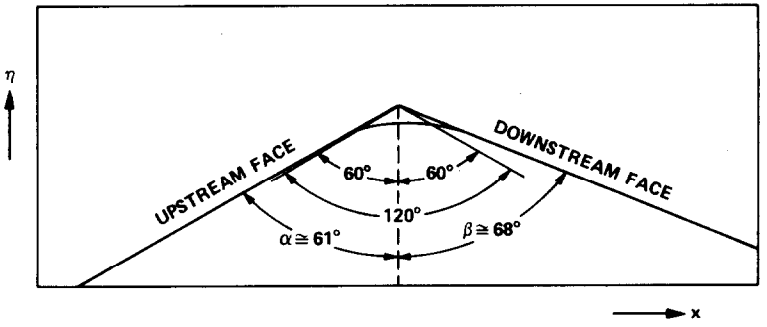

FIG. 7. Steepness of first downstream wave crest for $\mathrm{Fr} = 0.4$, $\delta = 0.0175$, $t = 3.3$.

characteristics: a sharpening of the crests, a broadening of the troughs, and a shortening of the wavelength compared to the linearized, analytic wave profile.

Figure 5 shows waves generated in time for $\mathrm{Fr} = 0.4$, $\delta = 0.02$. A steady state wave profile occurs at the pressure distribution at about $t = 2.7$. Of all cases considered, the steepest waves are generated by this case. Stokes [8] has shown that the limiting form of steady irrotational gravity waves is one with sharp crests containing an angle of 120°, that is, a maximum slope of 30°. At $t = 2.4$ in Fig. 5 at the first downstream crest $\alpha \cong 63°$ and $\beta \cong 73°$, these angles being those shown in Fig. 7 for another case. As this crest approaches a steady state, one expects α to be more nearly equal to β. These angles have been computed from numerical values for η in the immediate neighborhood of the crest peak and are only approximate, being rounded off to the nearest half degree. At $t = 3.0$, confidence in the accuracy of this crest is suspect because of the lack of resolution and the fact that α appears to be less than 60°, which is Stokes' lower limiting value. A little after $t = 3.6$ the solution breaks up at this peak. The Stokes limiting value of 120° is an upper limit for irrotational flow and, as pointed out in [17], " $\cdots$ it is very difficult, even in the laboratory, to generate a wave train that approaches this configuration. $\cdots$ the waves tend to become very unsteady as the curvature at the crest increases, so that even a small perturbation results in breaking." The experimental results of Salvesen [18] show that, for the case of a two-dimensional foil moving at constant speed below the free surface, the maximum slope and maximum wave elevation occurred at the first crest behind the foil and that, when breaking occurred, it started at this first crest. The largest slope ($90° - \alpha$ or β) without breaking reported in [18] is approximately 25°.

Figure 6 shows late time wave profiles for $\mathrm{Fr} = 0.4$ with $\delta = 0.01$, 0.0125, 0.015, 0.0175, and 0.02. Increasing δ results in greater nonlinearity of the wave profiles and increased sharpening of the crest angles. Figure 7 shows the crest angle for $\mathrm{Fr} = 0.4$, $\delta = 0.0175$ at $t = 3.3$.

Figure 8 shows time histories of wave resistance C_R, time rate of work $\dot{W}$, and time rate of energy dE/dt for $\mathrm{Fr} = 0.4$ with $\delta = 0.01$, 0.0125, 0.015, 0.0175, and 0.02. C_R and $\dot{W}$ are defined by Eqs. (16) and (15), respectively. dE/dt is the numerical time derivative of $KE + PE$, with KE and PE defined by Eqs. (13) and (14), respectively. Figure 8 shows that for all five cases Eq. (18) is satisfied after $t = 2.0$. For all five cases energy conservation, represented by Eq. (17), is pretty well satisfied up to $t = 2.0$. After $t = 2.0$, Eq. (17) is still reasonably satisfied except for the most nonlinear cases, in particular $\mathrm{Fr} = 0.4$ with $\delta = 0.0175$ and 0.02 which develop very sharp crests in time and have already been discussed. There is not enough resolution in these crests to accurately compute the integrands for KE (Eq. (13)) and PE (Eq. (14)), and since dE/dt is a numerical finite difference in time of $KE + PE$, the numerical errors are compounded in computing dE/dt. This also most likely explains some of the scatter of dE/dt.

Figure 9 shows a comparison between the steady state nonlinear numerical values of C_R and steady state analytic, linearized C_R for $\mathrm{Fr} = 0.4$ with various δ's. Although the difference between nonlinear and linear C_R is small, the difference increases with increasing δ. Factors that could cause a greater difference include decreasing the

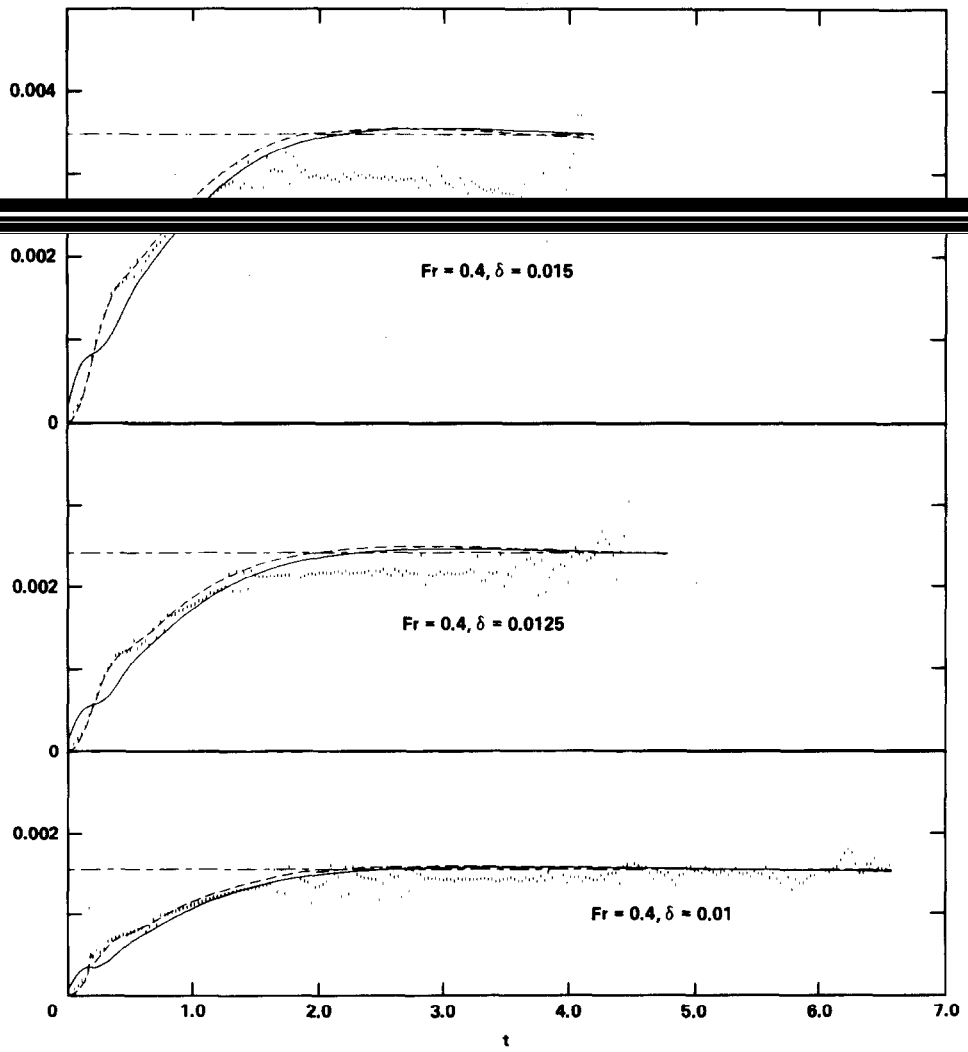

FIG. 8. Time histories of wave resistance C_R, time rate of work $\dot{W}$, and time rate of energy dE/dt for Fr = 0.4 with $\delta = 0.01$, 0.0125, 0.015, 0.0175, and 0.02. —, C_R; – – –, $\dot{W}$; '", dE/dt; — — —, linear, analytic, steady state value for C_R.

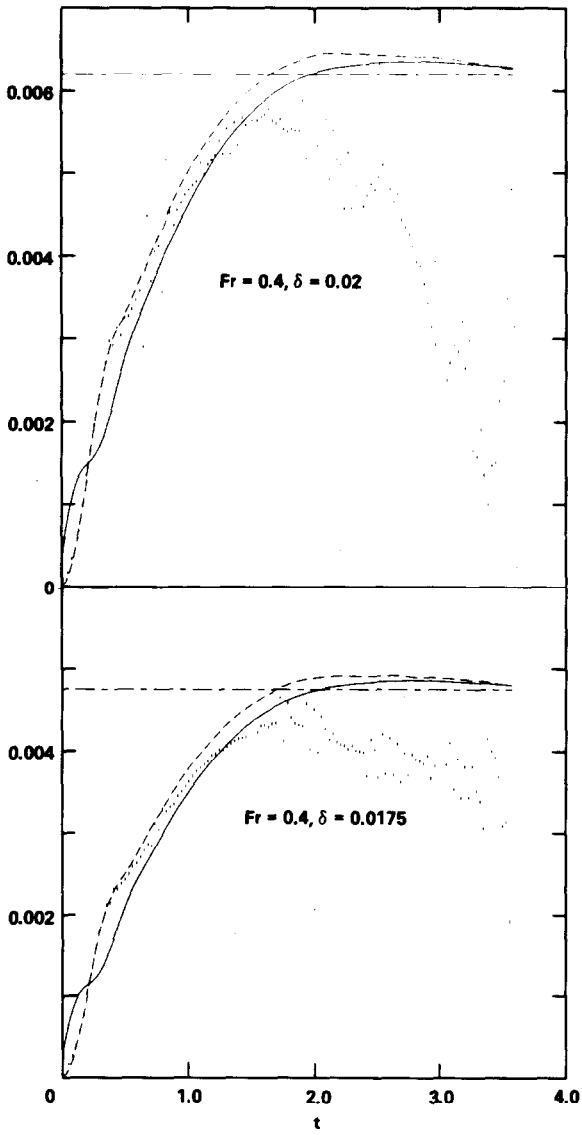

FIG 8—*Continued.*

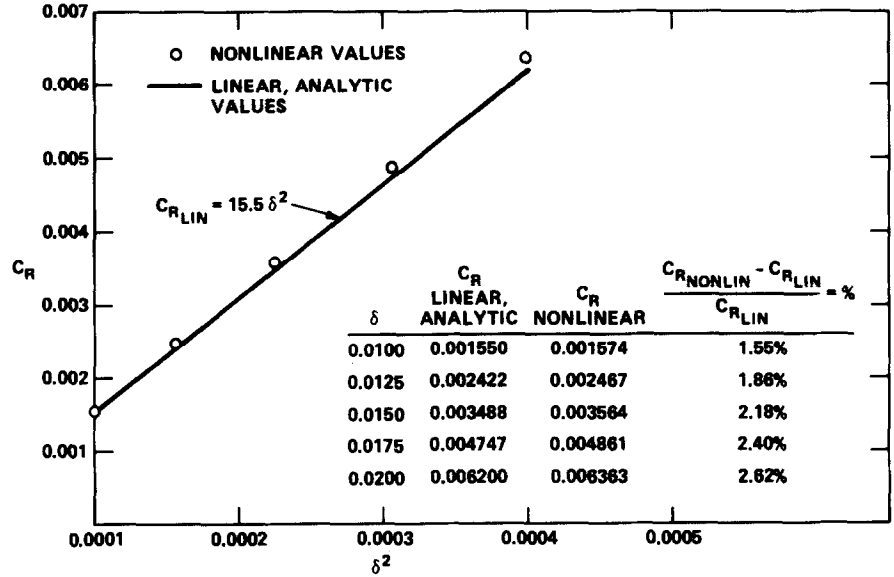

δ	C_R LINEAR, ANALYTIC	C_R NONLINEAR	$\frac{C_{R_{NONLIN}} - C_{R_{LIN}}}{C_{R_{LIN}}} = \%$
0.0100	0.001550	0.001574	1.55%
0.0125	0.002422	0.002467	1.86%
0.0150	0.003488	0.003564	2.18%
0.0175	0.004747	0.004861	2.40%
0.0200	0.006200	0.006363	2.62%

FIG. 9. Steady state wave resistance C_R versus δ^2 for Fr = 0.4.

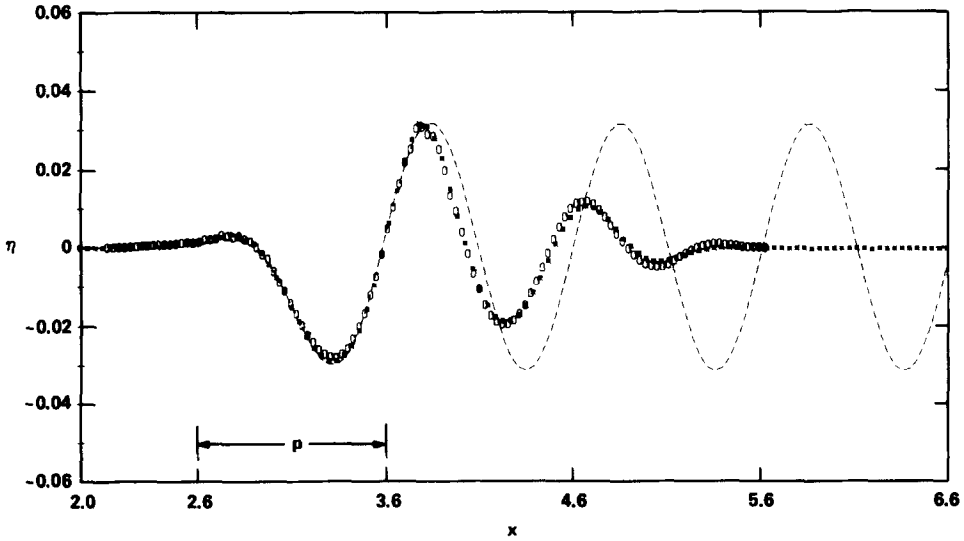

FIG. 10. Comparison of wave profiles on two different mesh spacings for Fr = 0.4, $\delta = 0.01$ at $t = 3.0$. ***, Mesh defined by Eqs. (31) and (32); ooo, finer mesh defined by Eqs. (31) modified and (32); – – –, linear, analytic, steady state solution.

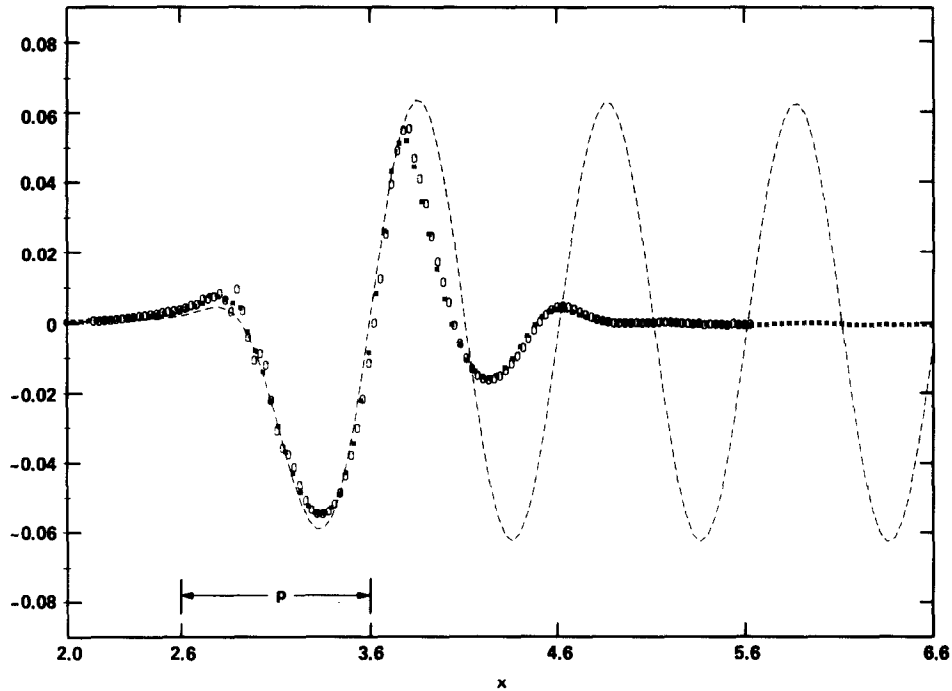

FIG. 11. Comparison of wave profiles on two different mesh spacings for $Fr = 0.4$, $\delta = 0.02$ at $t = 2.1$. ***, Mesh defined by Eqs. (31) and (32); ooo, finer mesh defined by Eqs. (31) modified and (32); – – –, linear, analytic, steady state solution.

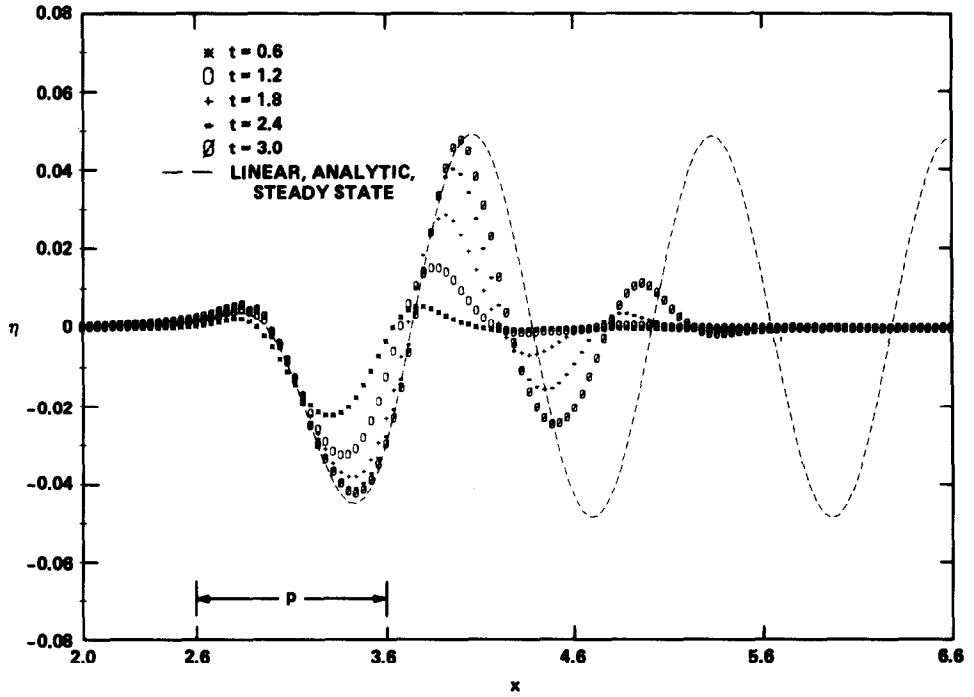

FIG. 12. Time sequence of waves generated for $Fr = 0.45$, $\delta = 0.015$.

depth h of the computational region in Fig 1a and changing the shape of the pressure distribution.

Figures 10 and 11 show a comparison of wave profiles computed on two different grids for the cases $\mathrm{Fr} = 0.4$, $\delta = 0.01$ at $t = 3.0$ and $\mathrm{Fr} = 0.4$, $\delta = 0.02$ at $t = 2.1$. The finer grid represented by circles, which is used only for Figs. 10 and 11, is given by Eqs. (31) and (32) with Δx in the fourth and fifth lines of Eq. (31) replaced by $\Delta x = 1.0/33.0$ and $\Delta x = 0.04$, respectively. This finer grid will be referred to as Eq. (31) modified in Figs. 10 and 11. The comparisons show good agreement. This finer grid seems adequate enough for comparison. Using a grid, for example, twice as fine (i.e., 50 grid intervals to represent the pressure distribution and twice as fine spacing near the pressure distribution) seems unnecessary and would incur much greater computer cost. The first downstream crest in Fig. 11 has $\alpha \cong 66°$ and $\beta \cong 76°$ replacing the angles in Fig. 7. The upstream or bow wave portion of the wave profile for $\mathrm{Fr} = 0.4$, $\delta = 0.02$ (which is the most extreme case considered in this paper) appears to require more than the very light filtering (Eq. (34)) that has been applied to it. This is also apparent in Fig. 6 for $\mathrm{Fr} = 0.4$, $\delta = 0.02$.

Figure 12 shows a time sequence of wave generation for $\mathrm{Fr} = 0.45$, $\delta = 0.015$. This larger Froude number produces a wavelength longer than those of the $\mathrm{Fr} = 0.4$ cases. Figure 13 shows a late time wave profile for this case.

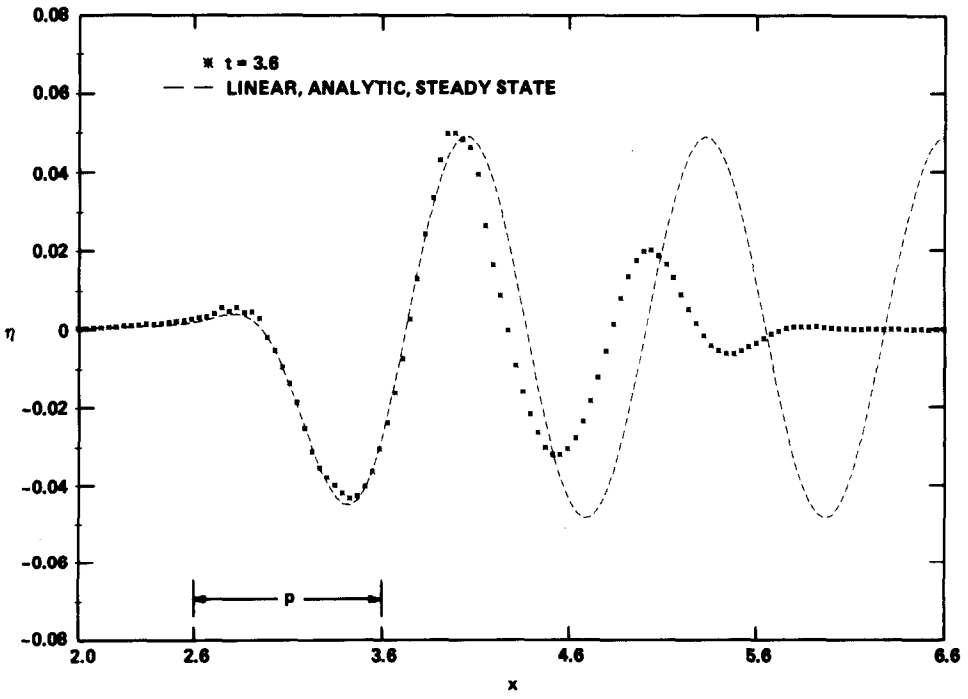

FIG. 13. Late time wave profile for $\mathrm{Fr} = 0.45$, $\delta = 0.015$ at $t = 3.6$.

In Figure 14 a time sequence of waves generated for $\mathrm{Fr} = 0.35$, $\delta = 0.0125$ is shown. The numerical solution at $t = 6.3$ is steady through the first two downstream crests. The wavelength measured from peak to peak of these crests is 0.72. The wavelength of the analytic, linearized solution is $2\pi \mathrm{Fr}^2 \cong 0.7697$. Thus the wavelength of the nonlinear numerical solution is 93.54% of the wavelength of the linearized solution, or 6.44% shorter. This is in good agreement with Salvesen's third-order perturbation theory [9], which states that

$$\lambda = 2\pi \mathrm{Fr}^2(1 - a^2/\mathrm{Fr}^4), \tag{38}$$

where λ is the nonlinear wavelength, a is the amplitude of the linearized solution far downstream, and $2\pi \mathrm{Fr}^2$ is the wavelength of the linearized solution. With $a = 0.0292$ for the present case, Eq. (38) predicts a nonlinear wavelength which is 94.32% of the wavelength for the linearized solution.

The numerical solution at $t = 6.3$ clearly shows the nonlinear features of a sharpening of the crests and a broadening of the troughs compared to the linearized solution. This is true of all the cases computed in this paper.

At $t = 6.3$ the first downstream crest has crest angles $\alpha \cong 71°$, $\beta \cong 72°$ and the second has $\alpha \cong 72°$, $\beta \cong 71°$. This case of $\mathrm{Fr} = 0.35$, $\delta = 0.0125$, along with $\mathrm{Fr} = 0.4$, $\delta = 0.01$, are the only cases of those considered in this paper that have been computed out to $t = 6.3$. It seems likely that these cases can be continued indefinitely but there is no reason to do so since the solution is already at steady state through the first two downstream wave crests. In the computation of the other cases which generate sharper crests the computations break down at the first downstream crest before the second crest is fully developed. This situation is in genereal agreement with the observations of physical experiments by Salvesen [18] and Banner and Philips [17] cited earlier.

In Fig. 15 time histories of C_R, $\dot{W}$, and dE/dt are shown for $\mathrm{Fr} = 0.45$, $\delta = 0.015$ and $\mathrm{Fr} = 0.35$, $\delta = 0.0125$. The linear, analytic C_R values are $C_R = 0.0017575$ for $\mathrm{Fr} = 0.35$, $\delta = 0.0125$ and $C_R = 0.0029502$ for $\mathrm{Fr} = 0.45$, $\delta = 0.015$.

Computer times used on the Texas Instruments Advanced Scientific Computer (TI-ASC) for each of the seven cases ranged from approximately 7 min, 8 sec for $\mathrm{Fr} = 0.4$, $\delta = 0.02$ to 11 min, 6 sec for $\mathrm{Fr} = 0.35$, $\delta = 0.0125$. The TI-ASC is approximately 25% faster than the IBM 360-91. The number of time steps per minute for each case with $\Delta t = 0.03$ ranged from approximately 23 time steps per minute for $\mathrm{Fr} = 0.4$, $\delta = 0.01$ to approximately 18 time steps per minute for $\mathrm{Fr} = 0.4$, $\delta = 0.02$. The average number of cycles per time step for all the cases was 3, with an average of 2 to 3 cycles per time step for $\mathrm{Fr} = 0.4$, $\delta = 0.01$ and $\mathrm{Fr} = 0.35$, $\delta = 0.0125$. The average number of Gauss–Seidel point iterations for the Laplace equation solution within each cycle was 1, with as many as 4 to 5 iterations required near $t = 0$.

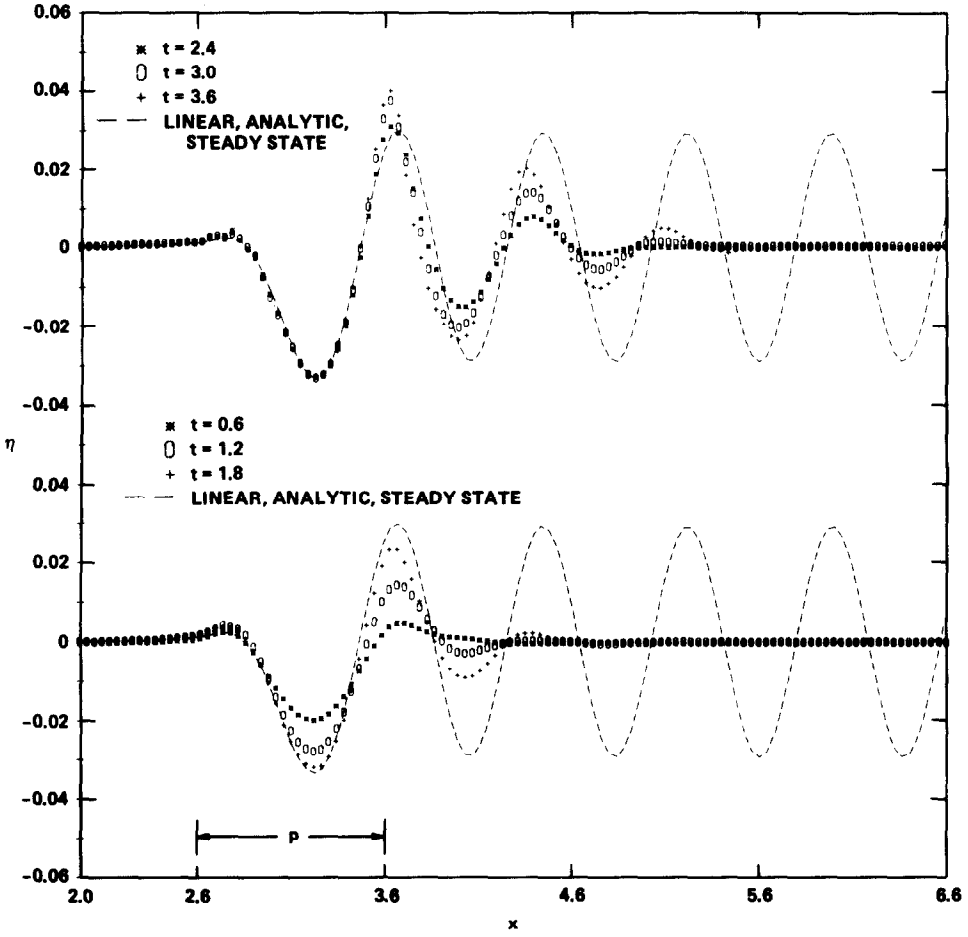

FIG. 14. Time sequence of waves generated for $\mathrm{Fr} = 0.35$, $\delta = 0.0125$.

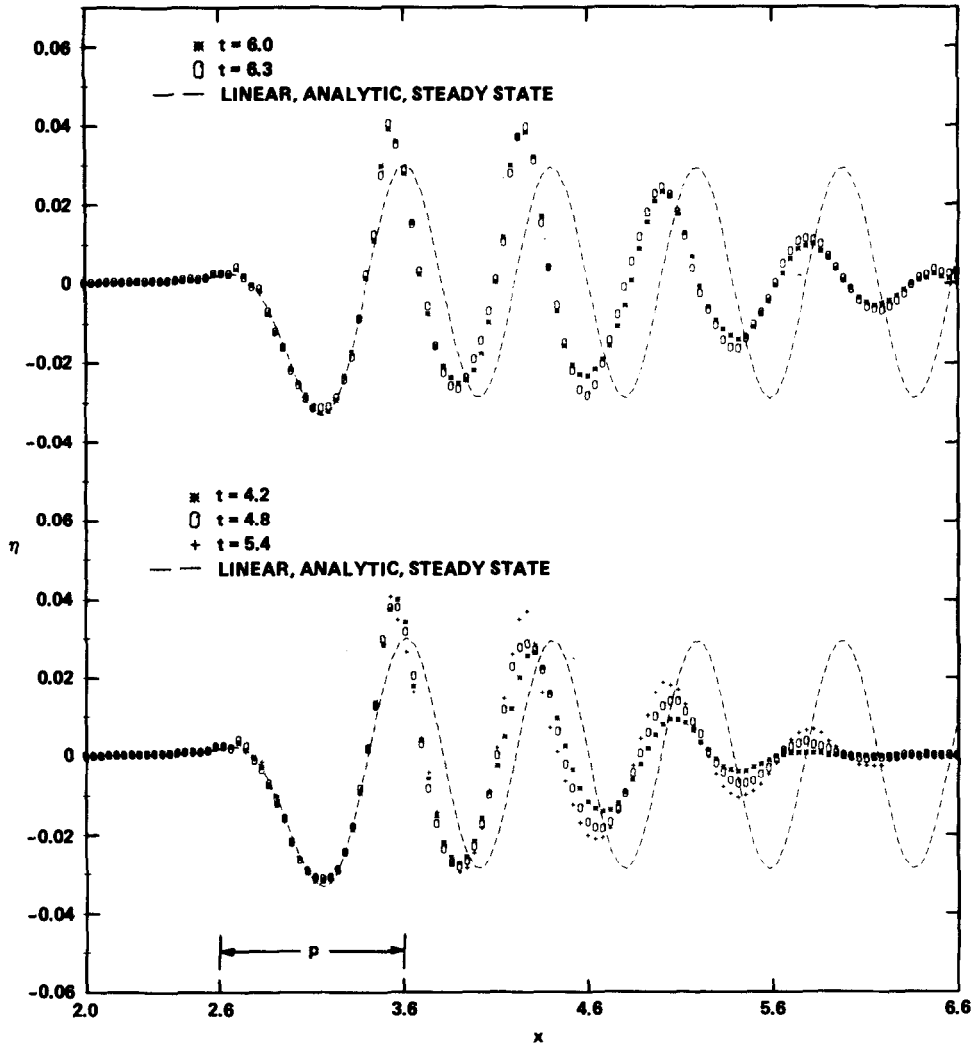

FIG. 14—*Continued.*

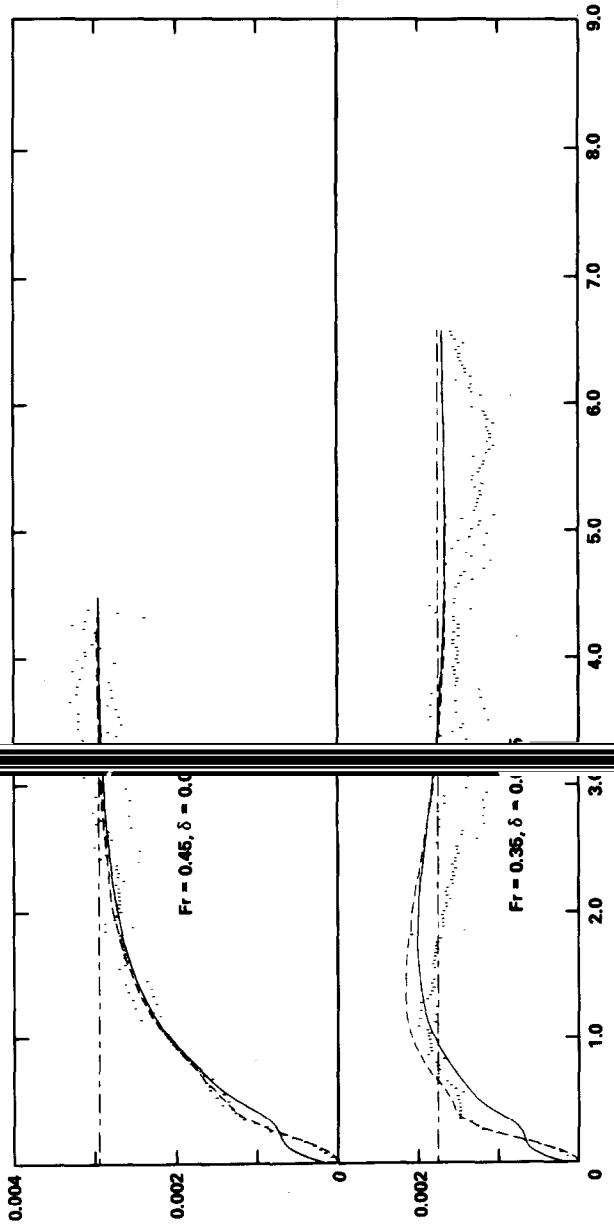

FIG. 15. Time histories of wave resistance C_R, time ... of work $\dot{W}$, and time rate of energy dE/dt for $\mathrm{Fr} = 0.35$, $\delta = 0.0125$ and $\mathrm{Fr} = 0.45$, $\delta = 0.015$. ——, C_R; – – –, $\dot{W}$; ", dE/dt; — — —, linear, ...lytic, steady state value for C_R.

5. Conclusions

The method of lines has been shown to be useful in computing the time dependent generation of nonlinear waves. Wave crests with sharpness approaching that of the limiting Stokes wave have been computed. The nonlinear waves obtained show sharpening of the wave crests, broadening of the wave troughs, and shortening of the wavelengths compared to linear theory. Steady state wave resistance has been obtained.

Acknowledgments

The author would like to thank Ms. Anne Laney for her careful typing of the manuscript. This work was supported by the Numerical Naval Hydrodynamics Program at the David W. Taylor Naval Ship Research and Development Center. This program is sponsored jointly by DTNSRDC and the Office of Naval Research.

References

1. C. H. von Kerczek and N. Salvesen, *in* "Proceedings, Tenth Symposium on Naval Hydrodynamics, Cambridge, Mass., June 24–28, 1974" (R. D. Cooper and S. W. Doroff, Eds.), pp. 649–663.
2. H. J. Haussling and R. T. Van Eseltine, *in* "Proceedings, First International Conference on Numerical Ship Hydrodynamics, Gaithersburg, Md., Oct. 20–22, 1975" (J. W. Schot and N. Salvesen, Eds.), pp. 295–313.
3. L. A. Kurtz, R. E. Smith, C. L. Parks, and L. R. Boney, *Comput. Fluids* **6** (1978), 49.
4. G. H. Meyer, *Numer. Math.* **29** (1978), 329.
5. G. H. Meyer, *J. Inst. Math. Appl.* **20** (1977), 317.
6. C. H. von Kerczek and N. Salvesen, *in* "Proceedings, Second International Conference on Numerical Ship Hydrodynamics, Berkeley, Calif., Sept. 19–21, 1977" (J. V. Wehausen and N. Salvesen, Eds.), pp. 292–300.
7. S. Ohring and J. Telste, *in* "Proceedings, Second International Conference on Numerical Ship Hydrodynamics, Berkeley, Calif., Sept. 19–21, 1977" (J. V. Wehausen and N. Salvesen, Eds.), pp. 88–103.
8. G. G. Stokes, *Proc. Cambridge Philos. Soc.* **4** (1883), 361–365.
9. N. Salvesen, *J. Fluid Mech.* **38** (1969), 415.
10. B. L. Buzbee, G. H. Golub, and C. W. Nielson, *SIAM J. Numer. Anal.* **7** (1970), 627.
11. M. J. Romanelli, *in* "Mathematical Methods for Digital Computers" (A. Ralston and H. S. Wilf, Eds.), p. 110, Wiley, New York, 1964.
12. M. S. Longuet-Higgins and E. D. Cokelet, *Poc. Roy. Soc. London Ser A* **350** (1976), 1.
13. R. Shapiro, *Math. Comput.* **29** (1975), 1094.
14. J. J. Stoker, "Water Waves," Interscience, New York, 1957.
15. J. V. Wehausen and E. V. Laitone, *in* "Encyclopedia of Physics" (S. Flügge and C. Truesdell, Eds.), Vol. 9, pp. 446–778, Springer–Verlag, Berlin, 1960.
16. L. J. Doctors and S. D. Sharma, *J. Ship. Res.* (1972), 248.
17. M. L. Banner and O. M. Phillips, *J. Fluid Mech.* **65** (1974), 647.
18. N. Salvesen, *in* "Office of Naval Research 6th Naval Hydrodynamics Symposium, Washington, D. C., 1966" pp. 595–636.